

Secondary cancer risk from modern external-beam radiotherapy of prostate cancer patients: Impact of fractionation and dose distribution

Chomporn Sitathane^{*}, Puangpen Tangboonduangjit, Mantana Dhanachai, Sawanee Suntiwong, Pornpan Yongvithisatid, Sukanya Rutchantuk, Pimolpun Changkaew, Rattana Watjiranon, Suphalak Khachonkham and Vipa Boonkitticharoen

Department of Diagnostic and Therapeutic Radiology, Faculty of Medicine Ramathibodi Hospital, Mahidol University, Bangkok 10400, Thailand

^{*}Corresponding author. Department of Diagnostic and Therapeutic Radiology, Ramathibodi Hospital, Mahidol University, Bangkok 10400, Thailand, E-mail: chomporn.sit@mahidol.ac.th

(Received 2 February 2021; revised 10 March 2021; editorial decision 2 April 2021)

ABSTRACT

Modern radiotherapy (RT) uses altered fractionation, long beam-on time and image-guided procedure. This study aimed to compare secondary cancer risk (SCR) associated with primary field, scatter/leakage radiations and image-guided procedure in prostate treatment using intensity-modulated RT (IMRT), CyberKnife stereotactic body RT (CK-SBRT) in relative to 3-dimensional conformal RT (3D-CRT). Prostate plans were generated for 3D-CRT, IMRT (39 fractions of 2 Gy), and CK-SBRT (five fractions of 7.25 Gy). Excess absolute risk (EAR) was calculated for organs in the primary field using Schneider's mechanistic model and concept of organ equivalent dose (OED) to account for dose inhomogeneity. Doses from image-guided procedure and scatter/leakage radiations were determined by phantom measurements. The results showed that hypofractionation relative to conventional fractionation yielded lower SCR for organs in primary field ($p \leq 0.0001$). SCR was further modulated by dose-volume distribution. For organs near the field edge, like the rectum and pelvic bone, CK-SBRT plan rendered better risk profiles than IMRT and 3D-CRT because of the absence of volume peak in high dose region (relative risk [RR]: 0.65, 0.22, respectively, $p \leq 0.0004$). CK-SBRT and IMRT generated more scatter/leakage and imaging doses than 3D-CRT ($p \leq 0.0002$). But primary field was the major contributor to SCR. EAR estimates (risk contributions, primary field: scatter/leakage radiations: imaging procedure) were 7.1 excess cases per 10^4 person-year (PY; 3.64:2.25:1) for CK-SBRT, 9.93 (7.32:2.33:1) for IMRT and 8.24 (15.99:2.35:1) for 3D-CRT ($p \leq 0.0002$). We conclude that modern RT added more but small SCR from scatter/leakage and imaging doses. The primary field is a major contributor of risk which can be mitigated by the use of hypofractionation.

Keywords: secondary cancer risk (SCR); intensity-modulated radiotherapy (IMRT); CyberKnife stereotactic body radiotherapy (CK-SBRT); primary field; scatter/leakage radiations; imaging dose

INTRODUCTION

Radiotherapy (RT) is an important treatment option for men who have localized prostate cancer, particularly those with intermediate to high risk diseases [1]. Treatment of prostate cancer with external-beam RT has evolved rapidly from the use of large field non-conformal RT to small field highly-conformal RT [2]. More recently, the modification of dose fractionation from conventional to hypofractionation [2] has been proposed for prostate cancer which has a smaller α/β of

1.5–2 Gy than the 3 Gy for late tissue complications [3]. Patient survival has been improved over time and the risk of secondary cancer has become a cause for concern.

The development of a secondary cancer is a serious, but uncommon, phenomenon which may take 10 or more years to develop [4]. Recent systemic reviews on secondary cancer induction after RT of prostate cancer suggest the increased secondary cancer risk (SCR) in the range of 1 in 220 to 1 in 290 [5, 6]. Most secondary cancers were

observed near the field edge, including carcinoma of the bladder, colon, rectum and also sarcoma in the treatment field [7–9]. The risk varies according to types of RT treatment. External-beam RT is consistently associated with an increased risk while brachytherapy, which includes minimal normal tissue in high dose volume, is not [6]. There is a common expectation that tightly targeted external-beam RT such as intensity-modulated RT (IMRT), focused-beam stereotactic body RT (SBRT) may reduce SCR. The reason behind such an expectation is that these techniques greatly reduce the volume of normal tissues (e.g. bladder and rectum) in the high dose region [10, 11]. In addition, modern RT techniques facilitate the safe use of hypofractionation which has been reported to be effective in prostate cancer treatment [12, 13] and may have theoretical potential in SCR reduction in comparing to conventional fractionation [14]. Whether the modern RT techniques will reduce the SCR is a subject of continued debate. Hall and Wu [15] expressed a concern on the potential increase in SCR upon the shift of 3-dimensional conformal RT (3D-CRT) to IMRT. Since delivery of a more conformal dose to the target volume involves using many more radiation fields thereby exposing a larger volume of normal tissues to low doses. Improved target coverage in modern RT techniques is achieved at the cost of higher out-of-field doses due to the use of longer beam-on time [15, 16]. Furthermore, these techniques greatly rely on image-guided procedures to facilitate accurate treatment delivery. Imaging technologies available to date vary from 2D-portal imaging to 3D-volumetric imaging. The procedures generate doses depending on specific protocols. Unlike the treatment field, the imaging beam is not target-focused and thereby generates doses widely, distributing across the patient volume [17]. Although the dose is small, it can contribute some risk to organs in or near the path of the treatment beam.

Due to the long latency for secondary cancer development, the evaluation of novel radiotherapeutic techniques usually relies on theoretical model prediction. A most widely-used hybrid model [18–21] developed by Schneider *et al.* [22] allows the estimation of organ-specific excess absolute risk (EAR) for patients with specified age at exposure and expected age attained. This model incorporates radiobiological relevant parameters (i.e. cell inactivation and cell repopulation during fractionation) to account for effect of dose fractionation and the rate of secondary cancer induction which is derived from the Hodgkin cohort in combination with the Japanese A-bomb survivors. The concept of organ equivalent dose (OED) is employed to take account of heterogeneous dose-volume distribution in modern RT.

The purposes of this study were 2-fold: (i) To assess the impact of dose fractionation (conventional fractionation used in IMRT and 3D-CRT versus hypofractionation delivered by CyberKnife stereotactic body RT [CK-SBRT]) and dose-volume distribution on SCR for in-field and near-field organs, and (ii) To assess and compare the SCR relevant to the primary field, scatter/leakage radiation and imaging procedures among RT techniques, including CK-SBRT, IMRT and 3D-CRT.

MATERIALS AND METHODS

This study assessed SCR from CK-SBRT, IMRT and 3D-CRT for patients with localized prostate cancer. Six patients had been chosen from a database of prostate cancer patients previously treated by CK-SBRT at Ramathibodi Hospital. The patients were selected as a representative group diagnosed with prostate cancer with different

tumour sizes. Three plans were created for each patient. The treatment plans are detailed in Table 1. Dosimetric data for SCR calculation were obtained from differential dose-volume histograms (dDVH) of the primary field. Doses from scatter/leakage radiations and imaging procedures were determined by phantom measurement using thermoluminescent dosimeters (TLD).

Treatment planning

Doses to organs at risk in the primary field were extracted from dDVH constructed by the treatment planning system (TPS): Eclipse TPS (Varian Medical Systems, Palo Alto, CA) for 3D-CRT and IMRT, Multiplan TPS (Accuray Incorporated, Sunnyvale, CA) for CK-SBRT. According to the guidance of the Radiation Therapy Oncology Group 0415 (RTOG 0415) [23], planning target volume (PTV) was contoured with a 7 mm (for 3D-CRT) or 8 mm (for IMRT) expansion around the clinical target volume (CTV), except the posterior direction toward the rectum where a 5 mm expansion was applied. For CK-SBRT plan, a 4 mm expansion was employed for the superior–inferior direction and 2 mm expansion for the rest. Doses to organs at risk of deterministic effects, including bladder, rectum, penile bulb and femoral heads, were within the tolerance doses specified for conventional fractionation and extreme hypofractionation [23]. For 3D-CRT and IMRT plans, the goal for target coverage was 100% of PTV receiving doses $\geq 95\%$ of prescription dose with the D_{\max} not exceeding 108%. In CK-SBRT, the goal was 100% of PTV receiving doses $\geq 80\%$ of prescribed dose and $D_{\max} \leq 110\%$.

Measurement of scatter/leakage doses

A phantom study was carried out to measure the scatter/leakage radiations generated during the primary treatment using TLD-700 rods ($^7\text{LiF,Mg,Ti}$) (Harshaw Chemical Company, Cleveland, OH). The scatter/leakage doses were determined for organs at distances more than 10 cm from the field edge. These organs included kidneys, stomach, liver, lungs, thyroid and brain. Locations and extents of the aforementioned organs in the RANDO[®] phantom were defined by a method using a 3D Cartesian coordinate system [24]. To measure organ doses, TLD rods were inserted into hole coordinates representing the organ centre. The prostate was irradiated according to the treatment plans described in Table 1. Doses for phantom irradiation were assigned as follows: 10 Gy of 6 MV photon for IMRT plan, 10 Gy of 10 MV photon for 3D-CRT and 5 Gy of 6 MV photon for CK-SBRT. The imaging system for target tracking in CK-SBRT was turned off during the measurement of scatter/leakage radiations. These measurements allowed the determination of Gy/MU used for the calculation of scatter/leakage doses to out-of-field organs.

Measurement of doses from imaging procedures

At our hospital, different imaging protocols were used to assure the accurate treatment delivery by 3D-CRT, IMRT and CK-SBRT (Table 2). The 3D-CRT is equipped with an electronic portal imaging device (EPID) to conduct the megavoltage (MV) portal imaging for the verification of field shape and setup procedure. For IMRT, verification of patient position and correction for target displacement were accomplished based on the information acquired by the on-board imager (OBI) which is capable of performing both the portal

Table 1. Treatment planning data for 3D-CRT, IMRT and CK-SBRT

Parameter	3D-CRT	IMRT	CK-SBRT
GTV, cm ³	47.8 (9.13) ^a	47.8 (9.13)	47.8 (9.13)
PTV, cm ³	112 (13.7)	126.8 (16)	85.1 (10.7)
Beam energy, MV	10	6	6
Prescribed dose, Gy	78	78	36.25
Dose per fraction, Gy	2	2	7.25
No. of fraction	39	39	5
Field/collimator size	8.3 × 7.1	9.8 × 7.6	15, 30
No. of beam orientation	7	9	250 (38)
Gantry angle, degree	0, 45, 95, 125, 236, 265, 315	0 to 320, 40° increment	NA
Maximum dose, Gy	81.27 (0.59)	81.8 (0)	45.22 (0.43)
Total treatment MU	11694 (573)	28379 (1691)	44262 (6414)
Imaging procedure	MV portal imaging	On-board imager (OBI) kV cone beam (CB) CT	Dual kV orthogonal imaging

^aData are presented as mean (SD) calculated for six patients.

and volumetric imaging. In CK-SBRT, treatment delivery was guided by the in-room dual X-ray imagers which tracked the intra-fraction tumour motion.

Organ doses from different imaging protocols (Table 2) were measured in phantom using TLD-700 rods for the MV beam and TLD-100H chips for the kV beam. Organs in dose measurement included those in the imaging portal, i.e. prostate, bladder, rectum, liver, stomach and kidneys. The phantom was exposed to the imaging beam with a number of frames (detailed in the last column of Table 2), just enough to generate thermoluminescent (TL) signals falling within the linear TL response.

Determination of secondary cancer risk

The SCR for organs in the primary field was calculated using a mechanistic model formulated by Schneider *et al.* [22]. The model incorporates parameters for cell killing (α') and cell repopulation (R) during fractionation yielding a dosimetry function termed risk equivalent dose (RED). The RED is derived for carcinoma risk:

$$\text{RED}_{\text{carcinoma}} = \frac{e^{-\alpha'D}}{\alpha'R} \left[1 - 2R + R^2 e^{\alpha'D} - (1 - R)^2 e^{\frac{-\alpha'RD}{1-R}} \right] \quad (1)$$

and also for sarcoma risk

$$\text{RED}_{\text{sarcoma}} = \frac{e^{-\alpha'D}}{\alpha'R} \left[1 - 2R + R^2 e^{\alpha'D} - (1 - R)^2 e^{\frac{-\alpha'RD}{1-R}} - \alpha'RD \right] \quad (2)$$

The cell killing parameter (α') as shown in equation (3) representing cells killed per dose fraction is defined by the linear quadratic (LQ) model.

$$\alpha' = \alpha \left[1 + \frac{d_T}{\alpha/\beta} \cdot \frac{D}{D_T} \right] \quad (3)$$

Equation (3) is formulated on the assumption that the normal tissue is irradiated with a fractionated treatment of equal dose fractions d up to a dose D . Where D_T and d_T are prescribed dose and dose per fraction to target volume. The α/β relevant to secondary cancer induction is 3 Gy for all tissue types [22]. By this mechanistic formulation, RED would allow risk assessment of different fractionation schemes.

Tissues closed to the primary field typically receive inhomogeneous doses. The concept of OED is employed to calculate the SCR for an organ exposed to heterogeneous doses [22]. By this approach, RED is weighted by its associated sub-volume $V(D_i)$. The summation over all voxel weighted RED values divided by the organ volume (VT) yields the OED:

$$\text{OED} = \frac{1}{V_T} \sum V(D_i) \cdot \text{RED}(D_i) \quad (4)$$

For doses from scatter/leakage radiations and imaging procedures, the dose response curves are considered linear. Therefore RED is proportional to physical dose D and the OED is estimated from the averaged organ dose [22].

EAR for a specific organ (the excess cases per 10 000 person-year [PY]) is the product of OED, initial slope of the dose-response curve (β , excess cases per 10⁴ PY-Gy) and a population dependent modifying function (μ) containing age at exposure (age x) and age attained (age a) variables (see equations [5] and [6]).

$$\text{EAR}_{\text{org}} = \frac{1}{V_T} \sum V(D_i) \cdot \beta \cdot \text{RED}(D_i) \cdot \mu(\text{age } x, \text{age } a) \quad (5)$$

$$\mu(\text{age } x, \text{age } a) = \exp[\gamma_e(\text{age } x - 30) + \gamma_a \ln(\text{age } a/70)]. \quad (6)$$

Organ-specific parameters for RED and EAR calculations were taken from the publication by Schneider *et al.* [22]. As described by the authors [22], the RED model parameters, α and R , for different tissues were obtained from the iterative fitting procedure (the best fits were defined at a coefficient of variation < 0.05) using the combined second cancer data from A-bomb survivors and Hodgkin's patients. To allow

Table 2. Imaging protocols for 3D-CRT, IMRT and CK-SBRT

Treatment technique	Imaging protocol	Field size, cm ³	Frequency/Duration	Images per measurement
3D-CRT	10 MV portal imaging Field shape • Gantry angle: 0, 45, 95, 125, 236, 315 degree • Image acquisition: One MU/frame, double exposure	8.3 × 7.1	One image weekly/seven weeks	Five frames
	Set up verification • AP, lateral projections • Image acquisition: 1 MU/frame, double exposure	8.3 × 7.1	One image pair weekly/eight weeks	Five frames/projection
IMRT	Positioning and setup verification kV CBCT • Scanning mode: half fan and full gantry rotation • No. of projections/scan: 655 • Image acquisition: 125 kV, 1mAs/projection	48 cm field of view, 16 cm length in scan volume	One scan daily, the first three days, one scan weekly, the next seven weeks	Five scans
	kV portal imaging • Image acquisition: AP, 75 kV, 16 mAs/frame	20 × 26	Two daily images/the first week Two images twice weekly/next seven weeks	40 frames
	Lateral, 105 kV, 80mAs/frame	20x26	Two daily images/the first week Two images twice weekly/next seven weeks	40 frames
CK-SBRT	Intrafraction tumour tracking • Dual X-ray orthogonal projection • Image acquisition: 120 kV, 10 mAs/projection	59 × 66	224 (176–255) daily projections/five days	150 projections

the comparative assessment of risks from the change in treatment plans, all EAR estimates were calculated for a representative patient irradiated at age 60 years and an attained age of 80 years [21]. Three different treatments were planned for each patient so as to allow treatment plan comparison independence of the inter-patient variabilities. By this design, differences in risk estimates between treatments were analysed by Student's paired t-test with $p \leq 0.05$ as a statistically significant level.

In plan evaluation, the prospect of changes in SCR with changes in treatment plans for a certain patient was evaluated in terms of relative risk (RR). However, it needs to be addressed here that the EAR estimate in this study did not serve the purpose to determine the absolute risks of SCR due to large uncertainties involving multiple model parameters in the EAR equation [22]. It was rather used for the comparison of treatment plans which were specified by the OED estimates incorporating the dose-volume histogram and altered fractionation scheme. Although the OED estimate is based on fewer parameters, it does not reflect the organ-specific cancer risk susceptibility β such as the

EAR estimate. Combining various organ risks from the primary beam component, scatter/leakage radiations and imaging procedure were performed on the EAR estimates rather than the OED estimates. For comparative treatment plan evaluation, this study only took account of uncertainties in dosimetric variables and variations in treatment delivery among six patients, uncertainty-associated model parameters were not included in the calculation [18–21].

RESULTS

Impact of dose-fractionation and dose-volume distribution on SCR

Two types of RED curves were generated by Schneider's mechanistic model, i.e. a bell-shaped curve for bladder carcinoma (Fig. 1a) and a plateau curve for rectal carcinoma, pelvic bone (Fig. 2a) and pelvic soft tissue sarcomas. Area under curve (AUC) which was the summation of RED values over the full dose range was calculated for

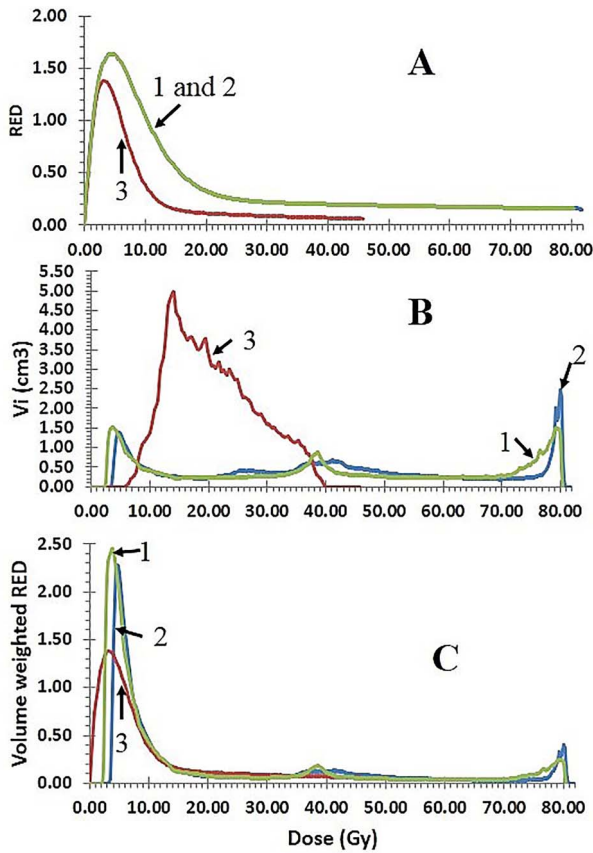


Fig. 1. Effects of fractionation and dose-volume distribution on SCR in bladder from 3D-CRT(1), IMRT(2) and CK-SBRT(3) plans. (A) RED curves; (B) dDVH; (C) Volume weighted RED curves.

organs in the primary field (Table 3). Hypofractionation treatment delivered by CK-SBRT yielded smaller AUC estimates for all organs than those from conventional fractionation used in 3D-CRT and IMRT.

Positive or negative dependence of SCR on doses was dictated by the inflection point (i.e. peak) of the RED curve. In low dose region before the curve reaching its peak, SCR increased with doses. Beyond its peak, the SCR decreased either rapidly (bell-shaped) (Fig. 1a) or slowly (plateau) with the increasing doses (Fig. 2a). For SCR with plateau type of dose response, the RED curve for sarcoma inflected at a higher dose than that for carcinoma. The bell-shaped curve (describing risk of bladder carcinoma) peaked at a much lower dose than the plateau curve (Table 3).

The SCR of an organ was further modulated by the dose-volume distribution. Adjusting the normal tissue volume to the low dose region away from the curve inflection could lower the SCR. In organs farther away from the beam edge, e.g. pelvic bone and soft tissue, the CK-SBRT plan displayed superior risk profiles by generating a single volume peak far below the RED curve inflection. This was in contrast to 3D-CRT and IMRT plans which generated multiple peaks distributing far below and also near the curve inflection (Fig. 2 and

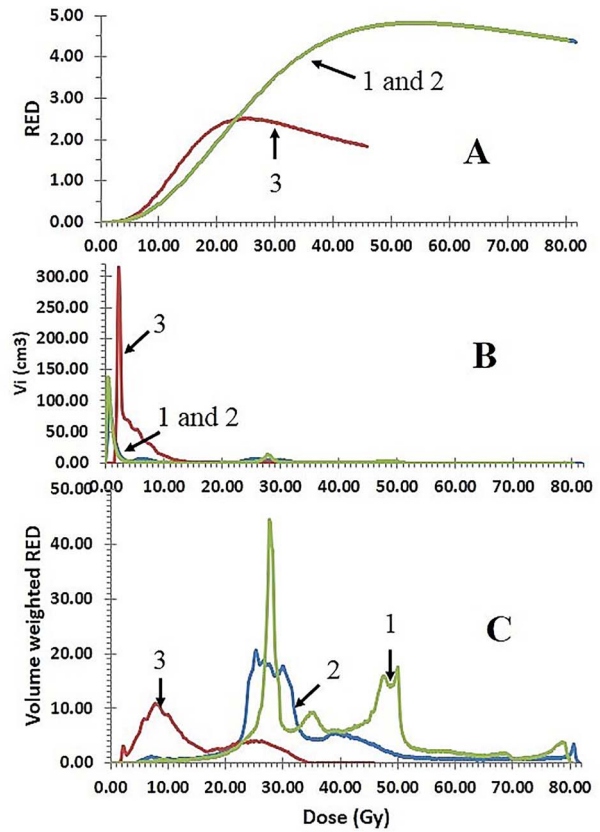


Fig. 2. Effects of fractionation and dose-volume distribution on SCR in pelvic bone from 3D-CRT(1), IMRT(2) and CK-SBRT(3) plans. (A) Risk-equivalent dose (RED) curves; (B) dDVH; (C) Volume weighted RED curves.

Table 3). For organs close to the field edge, like the rectum, 3D-CRT and IMRT plans generated volume peaks in low dose region and also in PTV. While CK-SBRT plan generated a single volume peak below the curve inflection, but the peak was broad with its tail smearing into the PTV (Table 3). As a consequence, SCR from CK-SBRT plan was lower than those of IMRT and 3D-CRT plans (Table 4). The bladder, another organ next to the prostate, had dose-volume distribution similar to that of the rectum but the risk profile was different because of its bell-shaped curve. Since the RED curve peaked at a much lower dose, all of the three plans generated volume peaks beyond the curve inflection where SCR decreased with the increasing doses (Fig. 1 and Table 3).

SCR estimates for the primary field, scatter/leakage radiations and imaging procedure

Estimates of OED and EAR for organs exposed to the primary field, scatter/leakage radiation and doses from the imaging procedures were determined and are presented in Tables 4–6.

Table 3. Characteristics of RED curves and corresponding dose volume distributions

	3D-CRT	IMRT	CK-SBRT
In-field soft tissue			
RED curve			
• AUC (Gy)	1422.1	1456.4	178.3
• Inflection point (Gy)	58.2	58.2	26.83
Tissue volume (Vt), cm ³	112	126.8	85.1
Peak (Gy) [Vp/Vt (%)]	80.27 [100]	79.57 [100]	40.48 [100]
Near-field soft tissue			
RED curve			
• AUC (Gy)	1422.1	1456.4	178.3
• Inflection point (Gy)	58.2	58.2	26.83
Tissue volume (Vt), cm ³	13154.8	13144.4	13359.5
Peak (Gy) [Vp/Vt (%)]			
1	0.2 [71.37]	0.333 [68.19]	2.26 [96.98]
2	6.77 [7.88]	4.03 [7.55]	–
3	25.73 [4.13]	23.77 [9.25]	–
Pelvic bone			
RED curve			
• AUC (Gy)	1350.4	1381.2	168.8
• Inflection point (Gy)	54	54	25.25
Tissue volume (Vt), cm ³	1270.8	1272.1	1287.6
Peak (Gy) [Vp/Vt (%)]			
1	0.267 [57.37]	0.4 [58.08]	2.26 [(95.27]
2	25.7 [5.64]	5.93 [8.84]	–
3	33.5 [6.94]	25.7 [12.54]	–
4	50.7 [6.29]	–	–
Rectum			
RED curve			
• AUC (Gy)	4004.4	4074.2	531
• Inflection point (Gy)	37.6	37.6	15.86
Tissue volume (Vt), cm ³	108.3	108.26	108.3
Peak, (Gy) [Vp/Vt (%)]			
1	2.5 [19.24]	3.37 [21.7]	7.25 [36.01]
2	79.38 [9.65]	79.4 [8.4]	–
Bladder			
RED curve			
• AUC (Gy)	154.8	155.9	29.23
• Inflection point (Gy)	4.4	4.4	3.17
Tissue volume (Vt), cm ³	155.1	155.09	155.1
Peak (Gy) [Vp/Vt(%)]			
1	2.53 [20.49]	3.57 [21.92]	–
2	79.55 [7.95]	79.83 [4.69]	13.05 [57.31]

The primary field

For sarcoma induction, the OED ratio (or denoted as RR) in relating CK-SBRT with either 3D-CRT or IMRT was calculated for in-field as 0.462 ($p \ll 0.0001$) and also 0.343 ($p \leq 0.0004$) for near-field soft tissue. In pelvic bone, the RR estimates were 0.223 ($p \ll 0.001$) when compared to 3D-CRT and 0.305 ($p = 0.0004$) to IMRT. For carcinoma induction (CK-SBRT vs 3D-CRT or CK-SBRT vs IMRT), the RR for rectum was 0.649 ($p \leq 0.0001$), while that for bladder was 0.519 ($p \ll 0.0001$). Comparisons between IMRT and 3D-CRT,

RR estimates for almost all sites were nearly equal to 1 except for the pelvic bone where the RR was 0.731 ($p < 0.0001$). The lower risk for the IMRT plan was due to a better dose-volume distribution, i.e. the absence of volume peak at high dose for the IMRT plan (Fig. 2 and Table 3). To account for the differences in organ carcinogenic susceptibility, OED was converted to EAR using the cancer induction rate (β) and the age modifying function (μ) derived from A-bomb data [22]. This allowed the summation of EAR estimates for all sites. Based on the total EAR values, SCR for CK-SBRT in

Table 4. OED and EAR estimates in associating with primary field calculated for CK-SBRT, IMRT and 3D-CRT plans

Organ	CK-SBRT		IMRT		3D-CRT	
	OED	EAR	OED	EAR	OED	EAR
	(Gy)	(10 ⁴ PY) ⁻¹	(Gy)	(10 ⁴ PY) ⁻¹	(Gy)	(10 ⁴ PY) ⁻¹
In-field						
• Pelvic soft tissue	2.28	0.86	4.93	1.86	4.93	1.86
Near field						
• Pelvic soft tissue	0.18	0.07	0.52	0.2	0.53	0.2
• Pelvic bone	0.29	0.04	0.95	0.12	1.3	0.16
• Rectum	5.51	1.88	8.6	2.94	8.4	2.87
• Bladder	0.35	0.9	0.67	1.71	0.68	1.72
All sites	–	3.75	–	6.83	–	6.81

Data are means. The %SD reflecting inter-patient variabilities had an average of 19.3% (range 10.3% – 29.9%).

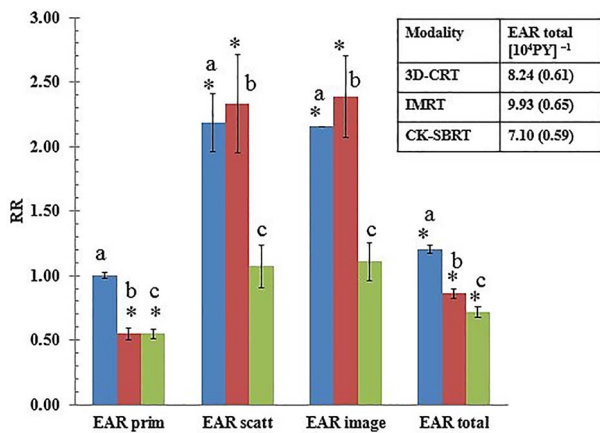


Fig. 3. Comparison of EAR estimates among treatment plans: CK-SBRT, IMRT and 3D-CRT in relevant to primary field, scatter/leakage radiations, image-guided procedure and total EAR. ^a IMRT/3D-CRT, ^b CK-SBRT/3D-CRT, ^c CK-SBRT/IMRT, * Denote significant difference.

relative to 3D-CRT or IMRT was 0.549 ($p \ll 0.0001$) (Table 4 and Fig. 3).

Scatter/leakage radiations

Doses from the scatter/leakage radiations, in principle, are proportional to the number of MU used in the treatment. On this basis, the estimates of MU ratio for CK-SBRT and IMRT in relative to 3D-CRT (Table 1) were 3.79 and 2.43, respectively. CK-SBRT in relative to 3D-CRT, the ratio of OED estimates were determined for kidney (0.832), stomach (1.75), liver (1.82) and lungs (2.74). These relative OED estimates were much smaller than the MU ratio of 3.79. Internal patient scatter in addition to treatment head scatter/leakage generated by the 3D-CRT plan could be the contributing factor. The evidence of patient scatter was confirmed by the observation of a decrease in OED with the increasing distance from the tumour geometric centre. This

observation was also recognized for the IMRT plan but not for the CK-SBRT plan. For distal organs such as the thyroid and brain where the internal scatter was minimal, the corresponding relative OED estimates were 4.52 and 4.23, respectively. These estimates were closer to the MU ratio of 3.79.

CK-SBRT plan in relative to IMRT, the relative OED estimates for thyroid (1.75) and brain (1.49) were in good agreement with the MU ratio of 1.56. For organs closer to the field edge where patient scatters were present, the estimates were smaller, i.e. lung 1.30, liver 0.826, stomach 0.81 and kidneys 0.374. Comparison between IMRT and 3D-CRT plans, the relative OED estimates for all sites were relatively constant with an average of 2.36 which was in good agreement with the MU ratio of 2.43.

When EAR estimates from all sites were combined, the RR values based on EAR were 2.32 (CK-SBRT vs 3D-CRT, $p = 0.0002$) and 1.07 (CK-SBRT vs IMRT, $p = 0.364$). IMRT in comparing to 3D-CRT, the RR was 2.17 ($p \ll 0.0001$) (Table 5 and Fig. 3).

Imaging procedures

Three treatment modalities employed different imaging technologies in set-up verification or tumour tracking, i.e. EPID for 3D-CRT; portal imaging and cone beam CT (CBCT) by kV OBI for IMRT; orthogonal imaging by in-room dual kV X-rays for CK-SBRT. Details for different imaging protocols are described in Table 2. All imaging procedures utilized broad beams and generated relatively uniform doses to organs located in or near the primary field. Referring to total EAR estimates in Table 6, the SCR for protocol used in CK-SBRT was 2.418 times greater than that of 3D-CRT ($p = 0.0001$) but was comparable to IMRT (RR = 1.104, $p = 0.31$). While an RR of 2.19 ($p \ll 0.0001$) was obtained for IMRT in relative to 3D-CRT (Table 6 and Fig. 3).

Combining the EAR estimates from all sources, i.e. primary field, scatter/leakage radiations and imaging procedure, yielded total EAR values of 7.1, 9.93 and 8.24 excess cases per 10⁴ PY for CK-SBRT, IMRT and 3D-CRT, respectively. Paired-sample Student's t-test rendered statistically significant conclusions which was independence of the inter-patient variabilities due to different tumour sizes. Risk contribution by the primary field, scatter/leakage radiations and imaging

Table 5. OED and EAR estimates in associating with scatter/leakage radiations calculated for CK-SBRT, IMRT and 3D-CRT plans

Organ	CK-SBRT		IMRT		3D-CRT	
	OED	EAR	OED	EAR	OED	EAR
	(Gy)	(10 ⁴ PY) ⁻¹	(Gy)	(10 ⁴ PY) ⁻¹	(Gy)	(10 ⁴ PY) ⁻¹
Out-of-field						
• Kidneys	0.139	—	0.372	—	0.167	—
• Stomach	0.098	0.616	0.121	0.767	0.056	0.355
• Liver	0.1	0.206	0.121	0.249	0.055	0.113
• Lung	0.096	1.432	0.074	1.113	0.035	0.517
• Thyroid	0.131	0.014	0.075	0.008	0.029	0.003
• Brain	0.11	0.052	0.074	0.034	0.026	0.012
All sites	—	2.32	—	2.17	—	1

Data are means. The %SD reflecting inter-patient variabilities had an average of 10.2% (range 2.7%–20.9%).

Table 6. OED and EAR estimates in associating with doses from image-guided procedures calculated for CK-SBRT, IMRT and 3D-CRT

Organ	CK-SBRT		IMRT		3D-CRT	
	OED	EAR	OED	EAR	OED	EAR
	(Gy)	(10 ⁴ PY) ⁻¹	(Gy)	(10 ⁴ PY) ⁻¹	(Gy)	(10 ⁴ PY) ⁻¹
In or near field						
• Pelvic soft tissue	0.17	0.064	0.259	0.098	0.16	0.06
• Rectum	0.091	0.031	0.222	0.076	0.109	0.037
• Bladder	0.326	0.829	0.274	0.696	0.129	0.329
Out-of-field						
• Kidneys	0.055	—	0.023	—	—	—
• Stomach	0.013	0.084	0.007	0.046	—	—
• Liver	0.012	0.025	0.009	0.018	—	—
All sites	—	1.03	—	0.933	—	0.426

Data are means. The %SD reflecting inter-patient variabilities had an average of 6.9% (range 2.6%–15.4%).

procedure were 3.64:2.25:1 for CK-SBRT, 7.32:2.33:1 for IMRT and 15.99:2.35:1 for 3D-CRT.

DISCUSSION

This study compared SCR associated with the primary field, scatter/leakage radiations and the image-guided procedure in prostate cancer treatment using modern external-beam RT including IMRT and CK-SBRT in relative to 3D-CRT. It appeared that the SCR from the primary field was the major contributor to the total risk which could be reduced by the use of hypofractionation. CK-SBRT in contrasting to 3D-CRT or IMRT using an extreme hypofractionation scheme (five fractions of 7.25 Gy) reduced the SCR for organs in the primary field by 50%. The organ-specific SCR was further modulated by dose-volume distribution. Adjusting the dose-volume distribution toward the low dose region resulted a reduction in SCR for organs with a plateau type of dose response. The dose-volume distribution for CK-SBRT was characterized by a single broad volume peak located at the low dose region while those for 3D-CRT and IMRT as multiple narrow volume peaks spanning across a relatively wide dose range. On this basis,

CK-SBRT plan yielded better risk profiles for near-field sarcoma and rectal carcinoma than those of 3D-CRT and IMRT plans.

Of special interest was the in-field soft tissue sarcoma induction where the risk was defined by the high dose portion of the plateau curve. In this setting, the hypofractionation in comparison to conventional fractionation could greatly reduce the sarcoma risk by more than 50%. Radiation-induced sarcoma has been a subject of recent concern. New epidemiological findings reveal the increased sarcoma risk in adulthood cancer survivors in addition to the long-been confirmed childhood cancer patients [25]. The use of hypofractionation treatment delivered by CK-SBRT would represent a feasible approach in minimizing the in-field sarcoma risk in prostate cancer patient which now tends to be treated at younger age and has a long life expectancy [26].

A few studies had evaluated the effect of altered fractionation on SCR using different mathematical models, i.e. competition model [27, 28] and LQ-based mechanistic model [14, 18, 21, 29]. No dose fractionation effect could be demonstrated by the study using competition model [28] in contrasting to those [14, 18, 21] using Schneider's mechanistic model [22] where differences in secondary cancer

induction between conventional and hypofractionation were reported. The competition model developed by Dasu *et al.* [27] predicts SCR on the ground of cell transformation and sterilization. This formulation yields a bell-shaped curve with a maximum risk at 5 Gy and a zero risk at dose above 20 Gy [27, 28]. With Schneider's model, the SCR is defined by cell initiation, inactivation and repopulation. By this approach, a bell-shaped curve is obtained for organ with minimal repopulation (i.e. small R) like the bladder [22]. In this study, we observed the curve for bladder carcinoma risk peaking at 4.4 Gy for conventional fractionation and 3.17 Gy for hypofractionation. Plateau curves were obtained for organs with large R and the curves peaked at much higher doses, i.e. 37.6–58.2 Gy for conventional fractionation and 15.86–25.25 Gy for hypofractionation. These model predictions were much more in consistence with several epidemiologic findings which revealed the persistence of risk at doses as high as 60 Gy [30]. The fractionation effect could also be demonstrated by a study using another model which incorporated cell repopulation [29]. It was postulated that more cells killed by the ablative dose fractions and less cell repopulation during a shorter treatment time were factors contributing to secondary cancer reduction observed in hypofractionation [14, 29].

The image-guided procedure has been an integral part of modern RT to aid accurate treatment delivery. Unlike the treatment field, the broad imaging beam traversed many more organs from in-field extending to a few organs farther away from the field edge. These organs included kidney, stomach and liver. Despite the use of different imaging techniques, i.e. MV portal imaging for 3D-CRT, portal and volumetric imaging for IMRT, doses to organs in the beam path were relatively uniform. For dual kV X-ray orthogonal imaging used in CK-SBRT, the dose to bladder was higher than other sites. Nevertheless, the imaging doses only added a small risk to the total SCR.

Regarding the out-of-field organs, the scatter/leakage radiations from IMRT and CK-SBRT plans generated comparable magnitudes of SCR but were greater than the risk posed by the 3D-CRT plan. Although IMRT treatment utilized fewer numbers of MU than the CK-SBRT plan, patient scatter from the IMRT plan generated extra doses and made the overall out-of-field risks comparable. Combining EAR estimates from all sources, i.e. primary field, scatter/leakage radiations and imaging procedure, yielded the total excess cases per 10^4 PY as follows: 8.24 for 3D-CRT, 9.93 for IMRT and 7.1 for CK-SBRT.

The overall SCR estimates obtained in this study were far less than the estimate of 35 excess cases per 10^4 PY reported by Liauw *et al.* [31]. The higher magnitude of SCR in Liauw's series could be accounted for by a number of confounding factors. As pointed out by the authors, a certain portion of patients with secondary bladder cancer had tobacco exposure as an etiological factor, while some with colorectal cancer were associated with a predisposing inflammation condition. In another comparative analysis of prostate brachytherapy versus prostatectomy, eight excess cases of bladder cancer per 10^4 PY were reported for both types of treatment [32]. It is well known that model prediction of absolute cancer risk for RT is associated with large uncertainties [22, 29] and must be viewed with caution.

This study has both strengths and limitations. Schneider's mechanistic model incorporates the LQ parameters relevant to cell

kill (α') and cell repopulation (R) for the calculation of RED. The LQ model has been widely used for prediction of cell survival from the conventional dose fraction of 1.8–2 Gy. The validity of LQ model has been challenged by the new concept of high dose radiobiology which describes the additional tumour cell killed by vascular damage and antitumor immunity [33]. This led to a question regarding the appropriateness of the RED estimates in predicting the SCR for CK-SBRT plan using an ablative dose fraction of 7.25 Gy. A recent study on the dependence of tumour control probability (TCP) on the biological effective dose (BED) using data from stage I non-small cell lung cancer either treated by 3D-CRT or SBRT. The study revealed that the pooled tumour control rates were satisfactorily fit to the sigmoidal TCP curve over a broad range of fraction sizes varying from < 2 Gy up to 18–20 Gy [34]. The monotonic increase in TCP with BED regardless the sizes of dose fraction (i.e. conventional or ablative fraction) suggests that the LQ model is adequate to explain the efficacy of SBRT [33, 34].

Schneider's mechanistic model serves as a convenient tool for comparative risk assessment of the contemporary RT modalities with unique dose distribution characteristics and using altered fractionation scheme. Like other models predicting cancer risk [29], this LQ-based model is known to be associated with large uncertainties [22, 35] that limit its use in the prediction of absolute cancer risk in RT. However, for the comparative risk assessment, the estimation of EAR for an organ of interest from a particular treatment plan, this and many other studies [18–21] did not include model parameter uncertainties in EAR calculation. Despite this weakness, we observed that EAR estimates from 3D-CRT plan for rectum (2.87 excess cases per 10^4 PY), bladder (1.72) and lung (0.52) calculated by Schneider's mechanistic model [22] were in line with epidemiological findings for 2D-RT reported by Brenner *et al.* [7]. In Brenner's report, the 10-year percentage increase in risk (RT vs surgery) for rectum, bladder and lung were 105, 77 and 42, respectively. The risk ratios between rectum and bladder were 1.36 for Brenner's study and 1.67 for this study. The lung which received scatter/leakage radiation showed a comparable risk as did near-field organs like the rectum and bladder. This observation might be explained on the basis of difference in susceptibility to cancer induction, i.e. the β value (excess cases per 10^4 PY-Gy). From A-bomb data, the β value for lung, bladder and rectum are 8.0, 3.8 and 0.73, respectively [21].

The primary field is the major contributor of SCR. Increased doses from scatter/leakage radiations and image-guided procedures observed in CK-SBRT and IMRT treatments do not substantially impact the total SCR. Hypofractionation treatment delivered by CK-SBRT induces lower SCR than conventional fractionation and may represent a feasible approach in SCR reduction. Modulation of dose-volume distribution by different treatment plans can influence organ-specific risk. In this regard, Schneider's cancer risk model may be used as a convenient tool in evaluation and optimization of treatment plans for modern external-beam RT so as to achieve the lowest possible risk of secondary cancer.

CONFLICT OF INTEREST

The authors declare they have no conflict of interest.

REFERENCES

1. Mohan R, Schellhammer PF. Treatment options for localized prostate cancer. *Am Fam Physician* 2011;84:413–20.
2. Martin NE, D'Amico AV. Progress and controversies: radiation therapy for prostate cancer. *CA Cancer J Clin* 2014;64:389–407.
3. Dasu A. Is the α/β value for prostate tumors low enough to be safely used in clinical trials? *Clin Oncol (R Coll Radiol)* 2007;19:289–301.
4. Ivanov VK, Gorsky AI, Kashcheev VV *et al*. Latent period in induction of radiogenic solid tumors in the cohort of emergency works. *Radiat Environ Biophys* 2009;48:247–52.
5. Murray L, Henry A, Hoskin P *et al*. Second primary cancers after radiation for prostate cancer: a systemic review of the clinical data and impact of treatment technique. *Radiother Oncol* 2014;110:213–28.
6. Wallis CJD, Mahar AL, Choo R *et al*. Second malignancies after radiotherapy for prostate cancer: Systemic review and meta-analysis. *BMJ* 2016;352:851–61.
7. Brenner DJ, Curtis RE, Hall EJ *et al*. Second malignancies in prostate carcinoma patients after radiotherapy compared with surgery. *Cancer* 2000;88:398–406.
8. Pickles T, Phillips N. The risk of second malignancy in men with prostate cancer treated with or without radiation in British Columbia, 1984–2000. *Radiother Oncol* 2002;65:145–51.
9. Moon K, Stukenborg GJ, Keim J *et al*. Cancer incidence after localized therapy for prostate cancer. *Cancer* 2006;107:991–8.
10. Newhauser WD, Durante M. Assessing the risk of second malignancies after modern radiotherapy. *Nat Rev Cancer* 2011;11:438–48.
11. Ng J, Shuryak I. Minimizing second cancer risk following radiotherapy: current perspectives. *Cancer Manage Res* 2015;7:1–11.
12. Katz AJ, Santoro M, Diblasio F *et al*. Stereotactic body radiotherapy for localized prostate cancer: disease control and quality of life at 6 years. *Radiat Oncol* 2013;8:118–25.
13. Bernetich M, Oliari C, Lanciano R *et al*. SBRT for the primary treatment of localized prostate cancer: the effect of Gleason score, dose and heterogeneity of intermediate risk on outcome utilizing 2.2014 NCCN risk stratification guide lines. *Front Oncol* 2014;4:312–8.
14. Schneider U, Besserer J, Mack A. Hypofractionated radiotherapy has the potential for second cancer reduction. *Theor Biol Med Model* 2010;7:1–6.
15. Hall EJ, Wu CS. Radiation-induced second cancers: the impact of 3D-CRT and IMRT. *Int J Radiat Oncol Biol Phys* 2003;56:83–8.
16. Purdy JA. Dose to normal tissues outside the radiation therapy patient's treated volume: a review of different radiation therapy techniques. *Health Phys* 2008;95:666–76.
17. Deng J, Zhang Y, Zhou L *et al*. Why are we concerned about imaging dose in the radiotherapy of cancers? *Austin J Radiol* 2014;1:1–3.
18. Paganetti H, Athar BS, Moteabbed MA *et al*. Assessment of radiation-induced second cancer risks in proton therapy and IMRT for organs inside the primary radiation field. *Phys Med Biol* 2012;57:6047–61.
19. Fuji H, Schneider U, Ishida Y *et al*. Assessment of organ dose reduction and secondary cancer risk associated with the use of proton beam therapy and intensity modulated radiation therapy in treatment of neuroblastomas. *Radiat Oncol* 2013;8:255–61.
20. Moteabbed M, Yock TI, Paganetti H. The risk of radiation-induced second cancers in the high to medium dose region: a comparison between passive and scanned proton therapy. IMRT and VMAT for pediatric patients with brain tumors. *Phys Med Biol* 2014;59:2883–99.
21. Murray LJ, Thompson CM, Lilley J *et al*. Radiation-induced second primary cancer risks from modern external beam radiotherapy for early prostate cancer: Impact of stereotactic ablative radiotherapy (SABR), volumetric moderated arc therapy (VMAT) and flattening filter free (FFF) radiotherapy. *Phys Med Biol* 2015;60:1237–57.
22. Schneider U, Sumila M, Robotka J. Site-specific dose-response relationships for cancer induction from the combined Japanese A-bomb and Hodgkin cohorts for doses relevant to radiotherapy. *Theor Biol Med Model* 2011;8:27–47.
23. Emami B. Tolerance of normal tissues to therapeutic radiation. *Reports Radiother Oncol* 2013;1:35–48.
24. Scalzetti EM, Huda W, Bhatt S *et al*. A method to obtain mean organ doses in RANDO phantom. *Health Phys* 2008;95:241–4.
25. Berrington de Gonzalez A, Kutsenko A, Rajaraman P. Sarcoma risk after radiation exposure. *Clin Sarcoma Res* 2012;2:18–25.
26. Li J, Djenaba JA, Soman A *et al*. Recent trends in prostate cancer incidence by age, cancer stage, and grade, the United States, 2001–2007. *Prostate. Cancer* 2012;2012:1–8.
27. Dasu A, Toma-Dasu I, Olofsson J *et al*. The use of risk estimation models for the induction of secondary cancers following radiotherapy. *Acta Oncol* 2005;44:339–47.
28. Dasu A, Toma-Dasu I, Franzen L *et al*. Secondary malignancies from prostate cancer radiation treatment: a risk analysis of the influence of the target margins and fractionation patterns. *Int J Radiat Oncol Biol Phys* 2011;79:738–46.
29. Shuryak I, Hahnfeldt P, Hlatky L *et al*. A new view of radiation-induced cancer: Integrating short- and long-term processes. Part II: second cancer risk estimation. *Radiat Environ Biophys* 2009;48:275–86.
30. Berrington de Gonzalez A, Gilbert E, Curtis R *et al*. Second solid cancers after radiation therapy: a systemic review of the epidemiologic studies of the radiation dose response relationship. *Int J Radiat Oncol Biol Phys* 2013;86:224–33.
31. Liauw SL, Sylvester JE, Morris CG *et al*. Second malignancies after prostate brachytherapy: incidence of bladder and colorectal cancers in patients with 15 years of potential follow-up. *Int J Radiat Oncol Biol Phys* 2006;66:669–763.
32. Hinnen KA, Schaapveld M, van Vulpen M *et al*. Prostate brachytherapy and second primary cancer risk: a competitive risk analysis. *J Clin Oncol* 2011;29:4510–5.
33. Brown MJ, Carison DJ, Brenner DJ. The tumor radiobiology of SRS and SBRT: are more than the 5 R's involved? *Int J Radiat Oncol Biol Phys* 2014;88:254–62.

34. Mehta N, King CR, Agazaryan N *et al.* Stereotactic body radiation therapy and 3-dimensional conformal radiotherapy for stage I non-small cell lung cancer: a pooled analysis of biological equivalent dose and local control. *Pract Radiat Oncol* 2012;2:288–95.
35. Nguyen J, Moteabbed M, Paganetti H. Assessment of uncertainties in radiation-induced cancer risk predictions at clinically relevant doses. *Med Phys* 2015;42:81–9 [PubMed: 25563249].